Confinement as a Determinant of Macromolecular Structure and Reactivity. II. Effects of Weakly Attractive Interactions between Confined Macrosolutes and Confining Structures

Allen P. Minton
Section on Physical Biochemistry, Laboratory of Biochemical Pharmacology, National Institute of Diabetes, Digestive and Kidney Diseases, National Institutes of Health, Bethesda, Maryland 20892 USA

ABSTRACT The effect of weak, nonspecific interaction between molecules confined within restricted elements of volume ("pores") and the boundary surfaces of the pore, upon the reactivity and physical state of the confined molecules, is explored by means of simple models. A confined molecule is represented by a rectangular parallelopiped having one of six orientations aligned with the cartesian coordinate axes, and the confining volume element is represented by a pair of parallel surfaces (planar pore), a tube of square cross section (square pore), or a cubical box (cubical pore). Weak interactions are modeled by square-well potentials having a defined range and well depth. Partition coefficients for distribution of molecules between the bulk and confined phase are calculated using an extension of the statistical-thermodynamic theory of Giddings et al. (1968). It is calculated that surface attraction with a potential of only a few kcal/mol monomer may result in large increases in the extent of self- or heteroassociation of confined molecules (as much as several orders of magnitude in favorable cases) linked to adsorption of the oligomeric species onto boundary surfaces. Calculations are also presented suggesting that surface attraction can lead to deformation of the native structure of adsorbed macromolecules. It is suggested that these findings are relevant to an understanding of the structure of eukaryotic cytoplasm.

INTRODUCTION

Electron micrographic studies have revealed that the cytoplasm of many types of eukaryotic cells is not a fluid continuum, but rather a two-phase, gel-like medium consisting of an aqueous fluid phase sequestered within a matrix of fibrous supramolecular structures including F-actin, microtubules, and intermediate filaments (Porter, 1984; Hirokawa, 1991). Depending upon the particular location within the cell, the fibers comprising the matrix may be preferentially oriented along a particular axis or may be randomly oriented. Macromolecular solutes within the aqueous phase thus are confined to elements of volume that may be described as pores, interstices, or channels between bounding elements of the fiber matrix. Electron micrographs indicate that pore dimensions are of the order of tens of nanometers, i.e., somewhat larger than individual protein molecules, but in the range of sizes expected of oligomeric aggregates of proteins. As the size of a confined macromolecule (or macromolecular aggregate) approaches the size of the confining volume element, considerations of volume exclusion dictate that the configurational entropy of the confined particle will be significantly reduced and its chemical potential correspondingly increased relative to the unbounded or bulk phase. In the previous paper of this series (Minton (1992), referred to hereafter as Part I), the effect of volume exclusion due to confinement upon a variety of hypothetical reactions taking place in model pores was explored, and it was concluded that confinement alone can profoundly influence reaction equilibria under conditions that might be realized in vivo.

A recent study (Lakatos and Minton, 1990) revealed that several proteins exhibit a tendency to form weak, nonspecific complexes with F-actin under conditions of moderate ionic strength. These weak complexes are characterized by standard free energies of formation of only a few RT per mole. Other proteins weakly self-associate under similar conditions at sufficiently high concentration (Muramatsu and Minton, 1989). Moreover, non-cross-linked collagen fibrils exhibit a spontaneous tendency to align in bundles, indicating the presence of a weakly attractive interaction between the collagen molecules in adjacent fibrils in solutions of moderate ionic strength (Leiken et al., 1994). Although the number of demonstrated examples is limited, the dissimilarity of proteins exhibiting such behavior is sufficiently great that we believe that the ability to participate in the formation of weak, nonspecific, and possibly transient complexes under quasi-physiological conditions may be a property of many, if not most, proteins.

In the present work, we investigate the influence of weakly attractive interactions between a confined particle (representing a globular protein) and the confining boundary on the equilibrium properties of the confined particle. It is shown that rather weak attractive interactions may profoundly influence the reactivity and conformation of confined molecules.

Received for publication 14 November 1994 and in final form 20 January 1995.

Address reprint requests to Dr. Allen P. Minton, Section on Physical Biochemistry, Laboratory of Biochemical Pharmacology, National Institute of Diabetes, Digestive and Kidney Diseases, Building 8, Room 226, National Institutes of Health, Bethesda, MD 20892. Tel.: 301-496-3604; Fax: 301-402-0240; E-mail: minton@helix.nih.gov.

0006-3495/95/04/1311/12 $2.00

DESCRIPTION OF MODEL AND CALCULATIONS

As in Part I, the effect of confinement and interaction upon the equilibrium constant for a specified reaction is calculated according to

$$\Gamma \equiv K^{\text{pore}}/K^{\text{bulk}} = \prod_{\text{products}} \mathbf{K}_i^{n_i} \Big/ \prod_{\text{reactants}} \mathbf{K}_i^{n_i}, \qquad (1)$$

where K^{pore} and K^{bulk} are the equilibrium constants of the reaction in the pore (bounded) and bulk (unbounded) phases, respectively, $\mathbf{K}_i$ is the equilibrium coefficient for partition of the ith species between the bulk and pore phases ($\equiv c_i^{\text{pore}}/c_i^{\text{bulk}}$), and n_i is the stoichiometric coefficient of the ith species in the specified reaction.

Equilibrium partition coefficients are calculated according to (Giddings et al., 1968):

$$\mathbf{K}_i \equiv \frac{c_i^{\text{pore}}}{c_i^{\text{bulk}}} = \frac{\int\int \exp[-U_i(\phi, r)/k_B T]\, d\phi\, dr}{\int\int d\phi\, dr}, \qquad (2)$$

where c_i^{pore} and c_i^{bulk} denote the concentrations of the ith species in the pore and bulk phases respectively, $U_i(\phi, r)$ denotes the potential energy of interaction between a particle of the ith species and the confining boundaries as a function of the orientational and positional coordinates of the particle, denoted by ϕ and r, respectively, k_B is Boltzmann's constant, and T is the absolute temperature.

For the purpose of the present investigation, a bounded volume element is modeled by a rectangular parallelopiped (PP) with sides of length $2r_{px}$, $2r_{py}$, and $2r_{pz}$, centered at the origin of a set of Cartesian coordinates. The pore is thus bounded by planes parallel to the yz axis at $+r_{px}$ and $-r_{px}$, by planes parallel to the xz axis at $+r_{py}$ and $-r_{py}$, and by planes parallel to the xy axis at $+r_{pz}$ and $-r_{pz}$. A confined particle is modeled by a rectangular PP with sides of length $2r_a$, $2r_b$, and $2r_c$. Because of the nature of the model interactions to be introduced, the particle is restricted to the six orientations in which the sides of the PP are parallel or perpendicular to the Cartesian coordinate axes. Thus, the generalized orientational coordinate ϕ reduces to a set of six discrete orientations, and Eq. 2 reduces to

$$\mathbf{K}_i = \frac{\sum_{j=1}^{6} \int \exp[-U_i(\phi_j, r)/k_B T]\, dr}{6 \int dr}, \qquad (3)$$

where $U_i(\phi_j, r)$ denotes the potential of a particle of the ith species at position r in the jth orientation. A specific point in configurational space will be denoted as follows. Let the particle be situated such that its center of mass lies at the point (r_x, r_y, r_z), with the i axis in the x direction, the j axis in the y direction, and the k axis in the z direction, where the indices i, j, and k represent permutations of a, b, and c. This configuration is denoted by $\{r_x, r_y, r_z, i, j, k\}$.

CALCULATION OF THE POTENTIAL ENERGY OF A CONFIGURATION

In Part I, interactions between the confined particle and the confining boundary were assumed to be of the hard particle type, i.e., for a given set of positional and orientational coordinates, if a particle falls entirely within the confined region, the potential is 0, otherwise infinite. In the present work, interactions between a confined particle and the confining boundary are modeled by a set of square-well potentials defined by the distance between each face of the confined particle and the planar boundary that it opposes.

The potential energy of the configuration $\{r_x, r_y, r_z, i, j, k\}$, denoted by $U(r_x, r_y, r_z, i, j, k)$, is given by the sum of potential energies associated with each face of the confined PP and the corresponding boundary. There are six such contributions, but we shall pair within a single term interactions associated with the two opposite faces of the confined PP normal to a given axial direction, leading to a decomposition of the total potential into three terms associated with each of the coordinate axes:

$$U(r_x, r_y, r_z, i, j, k) = U_1(r_x, i) + U_1(r_y, j) + U_1(r_z, k). \qquad (4)$$

Let m represent one of the three axial directions (x, y, or z); r_m denotes the m coordinate of the center of the confined PP. Let t represent the axis of the confined PP parallel to the m axis of the pore (i.e., $t = i, j$, or k); $2r_t$ equals the length of the confined PP in the direction of the m axis. Finally, let u and v represent the other two edges perpendicular to the m axis; the two $\{uv\}$ faces of the confined PP are normal to the m axis. Then $U_1(r_m, t)$ represents a "one-dimensional" contribution to the total potential energy, arising from interactions of the $\{uv\}$ faces of the confined particle with the two boundaries normal to the m axis.

U_1 is evaluated as follows. Let d represent the "range" of the square-well interaction, such that if a face of the confined particle lies within a distance d of the confining boundary, an energy of interaction proportional to the area of the particle face must be taken into account in calculating the total potential energy. Depending upon the relative magnitudes of r_t, r_{pm}, and d, four possible cases, illustrated in Fig. 1, ensue:

Case I: $r_t \le (r_{pm} - d)$. Depending upon the value of r_m, neither or one of the two $\{uv\}$ faces of the particle may interact with a boundary surface.

$$U_1(r_m, t) = \begin{cases} 0 & 0 \le r_m < (r_{pm} - r_t - d) \\ W_{uv} k_B T & (r_{pm} - r_t - d) \le r_m < (r_{pm} - r_t) \\ \infty & r_m \ge (r_{pm} - r_t) \end{cases} \qquad (5)$$

where W_{uv} is an interaction energy proportional to the area of the $\{uv\}$ face of the PP, i.e. $W_{uv} \equiv W \cdot r_u \cdot r_v$, where W is a constant of proportionality.

Case II: $(r_{pm} - d) < r_t \le (r_{pm} - d/2)$. Depending upon the value of r_m, one or both $\{uv\}$ faces of the particle may

interact with boundary surfaces.

$$U_1(r_m, t) = \begin{cases} 2W_{uv}k_BT & 0 \le r_m < (r_t - r_{pm} + d) \\ W_{uv}k_BT & (r_t - r_{pm} + d) \le r_m < (r_{pm} - r_t) \\ \infty & r_m \ge (r_{pm} - r_t) \end{cases} \quad (6)$$

Case III: $(r_{pm} - d/2) < r_t \le r_{pm}$. Both $\{uv\}$ faces interact with the boundaries.

$$U_1(r_m, t) = \begin{cases} 2W_{uv}k_BT & 0 \le r_m < (r_{pm} - r_t) \\ \infty & r_m \ge (r_{pm} - r_t) \end{cases} \quad (7)$$

Case IV: $r_t > r_{pm}$. Both $\{uv\}$ faces intersect the boundaries.

$$U_1(r_m, t) = \infty \quad (8)$$

CALCULATION OF THE PARTITION COEFFICIENT

Equation 3 may be expanded as

$$K_i = \frac{I_3(a,b,c) + I_3(a,c,b) + I_3(b,a,c) + I_3(b,c,a) + I_3(c,a,b) + I_3(c,b,a)}{6\, r_{px} r_{py} r_{pz}}, \quad (9)$$

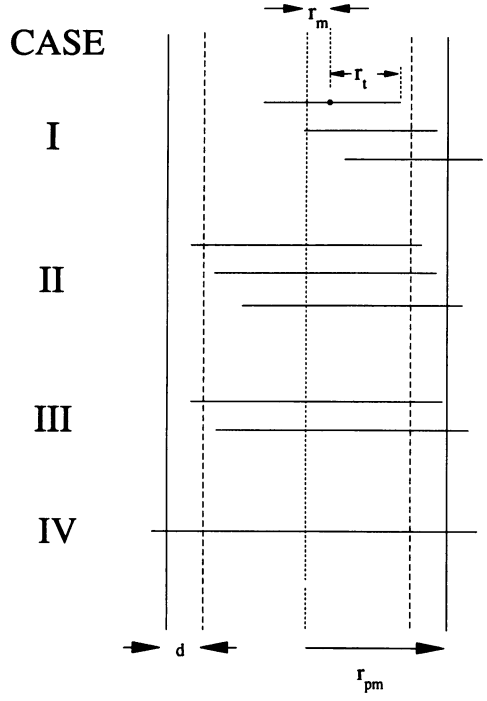

FIGURE 1 Schematic illustration of possible cases for interactions in one dimension. The ends of the horizontal lines represent the positions of the {uv} faces of the confined parallelopiped relative to the boundaries of the pore, defined as planes normal to the m axis at $\pm r_{pm}$. The several horizontal lines drawn for a particular case represent subcases described in Eqs. 5–7. If the end of the line lies between the center of the pore and the two dotted lines lying at a distance d from the boundary, no interaction between that face and the boundary exists. If the end of the line lies between the dotted line and the pore boundary, an interaction with the potential specified in the text exists. If the end of the line lies outside of the pore boundary, then an interaction having infinite potential (i.e., a "forbidden" configuration) exists.

where

$$I_3(i,j,k) \equiv \int dr_x \int dr_y \int dr_z \exp\left[-\frac{U(r_x, r_y, r_z, i, j, k)}{k_BT}\right].$$

The species index i has been dropped from the right-hand side of Eq. 9 to eliminate confusion with the dummy index i appearing in the subsequent definition of I_3. However, it should be clear that the arguments a, b, and c on the right-hand side of Eq. 9 refer specifically to orientations and dimensions of the confined particle of species i. It follows from Eq. 4 that

$$I_3(i,j,k) = I_1(x,i) \times I_1(y,j) \times I_1(z,k), \quad (10a)$$

where

$$I_1(m,t) \equiv \int_0^{r_{pm}} dr_m \exp\left[-\frac{U_1(r_m, t)}{k_BT}\right]. \quad (10b)$$

For each of the four geometric possibilities delineated above, the following results are derived from Eqs. 5–8 and 10b.

Case I:

$$I_1(m,t) = r_{pm} - r_t + d[\exp(-W_{uv}) - 1] \quad (11)$$

Case II:

$$I_1(m,t) = \exp(-2W_{uv})(r_t - r_{pm} + d) + \exp(-W_{uv})(2r_{pm} - 2r_t - d) \quad (12)$$

Case III:

$$I_1(m,t) = \exp(-2W_{uv})(r_{pm} - r_t) \quad (13)$$

Case IV:

$$I_1(m,t) = 0 \quad (14)$$

CALCULATION OF PARTITION COEFFICIENTS FOR SPECIFIC PORE MODELS

Planar pore model (r_{py}, $r_{pz} \to \infty$)

It follows from the definitions of $I_1(m,t)$ and $I_3(i,j,k)$ given in Eqs. 10 and 9 above that

$$\lim_{r_{pm}\to\infty} \frac{I_1(m,t)}{r_{pm}} = 1 \quad (15)$$

and

$$\lim_{r_{py}, r_{pz}\to\infty} \frac{I_3(i,j,k)}{r_{px} r_{py} r_{pz}} = \frac{I_1(x,i)}{r_{px}} \quad (16)$$

Thus, for the planar pore model, Eq. 9 reduces to

$$K_i = \frac{I_1(x,a) + I_1(x,b) + I_1(x,c)}{3r_{px}}. \quad (17)$$

Square pore model ($r_{pz} \to \infty$, $r_{px} = r_{py}$)

Because $r_{px} = r_{py}$, $I_1(x,t) = I_1(y,t)$, and it follows from Eqs. 10 and 15 that

$$\lim_{r_{pz}\to\infty} \frac{I_3(a,b,c)}{r_{px} r_{py} r_{pz}} = \frac{I_2(a,b)}{r_{pz}^2}, \quad (18)$$

where $I_2(a, b) \equiv I_1(x, a) \cdot I_1(x, b)$. Then Eq. 9 reduces to

$$\mathbf{K}_i = \frac{I_2(a, b) + I_2(a, c) + I_2(b, c)}{3r_{px}^2} \quad (19)$$

Cubical pore model ($r_{px} = r_{py} = r_{pz}$)

It follows from the equality of all pore dimensions that

$$I_1(x, t) = I_1(y, t) = I_1(z, t)$$

and

$$I_3(i, j, k) = I_1(x, i) \cdot I_1(x, y) \cdot I_1(x, z) = I_3(\{i, j, k\}),$$

i.e., the value of I_3 is independent of the ordering of the arguments i, j, and k. Hence, Eq. 9 reduces to

$$\mathbf{K}_i = \frac{I_3(a, b, c)}{r_{px}^3}. \quad (20)$$

The planar, square, and cubical pore models are illustrated in Fig. 2 *a–c*, respectively, of Part I.

RESULTS AND DISCUSSION

Macromolecular self-association

Consider the reaction $nA \rightleftharpoons A_n$, with an equilibrium constant in the bulk (unconfined) phase

$$K_n^{bulk} \equiv c_n^{bulk}/(c_1^{bulk})^n$$

and an equilibrium constant in the pore (confined volume element)

$$K_n^{pore} \equiv c_n^{pore}/(c_1^{pore})^n$$

For this reaction, Eq. 1 reduces to

$$\Gamma \equiv \frac{K_n^{pore}}{K_n^{bulk}} = \frac{\mathbf{K}_n}{\mathbf{K}_1^n}. \quad (21)$$

In the present model, monomer was represented as a cube with edges of halflength (pseudo-radius) r_1 and volume $V_1 = 8r_1^3$. An n-mer was represented by three differently shaped particles, all with $V_n = nV_1$. The "compact" n-mer was represented by a cube with edges of halflength $r_n = n^{1/3}r_1$; the "rod-like" n-mer was represented by a PP with edges of halflength r_1, r_1, nr_1; and the "plate-like" n-mer was represented by a PP with edges of halflength r_1, $n^{1/2}r_1$, $n^{1/2}r_1$.

Hard particle interactions

Initial calculations of the effect of confinement upon Γ were carried out in the hard particle approximation ($W_{UV} = 0$) to assess the effect of discretizing orientational configurations, and to establish a reference for comparison with interacting systems. In Fig. 2 *A* the calculated value of log Γ in a planar pore is plotted as the ratio of r_1:r_{px} for several values of n and for the three differently shaped n-mers described above. These results may be compared with earlier results presented in Part I, replotted in Fig. 2 *B*, which were obtained by modeling the monomer as a sphere and the n-mer as a larger sphere, a spherocylinder, or a torocylinder, with all possible orientations taken into account. It may be seen that despite the many differences in detail between the two models, the results agree qualitatively, and in some cases semiquantitatively, for $r_1/r_{px} \lesssim 0.6$, indicating that under these conditions (1) discretization of orientations does not qualitatively perturb the orientational contribution to the configurational integral (i.e., the rotational entropy), and that (2) details of shape specification do not qualitatively affect translational and orientational contributions to the configurational integral. Hence, one may have some confidence that simplifications introduced into the model to make it analytically soluble do not qualitatively change its thermodynamic properties.

Interacting systems

Consider a cubical monomer with pseudo-radius r_1. We define an interaction parameter $W_1 \equiv 4Wr_1^2$, representing the potential of interaction of a single monomer interacting with

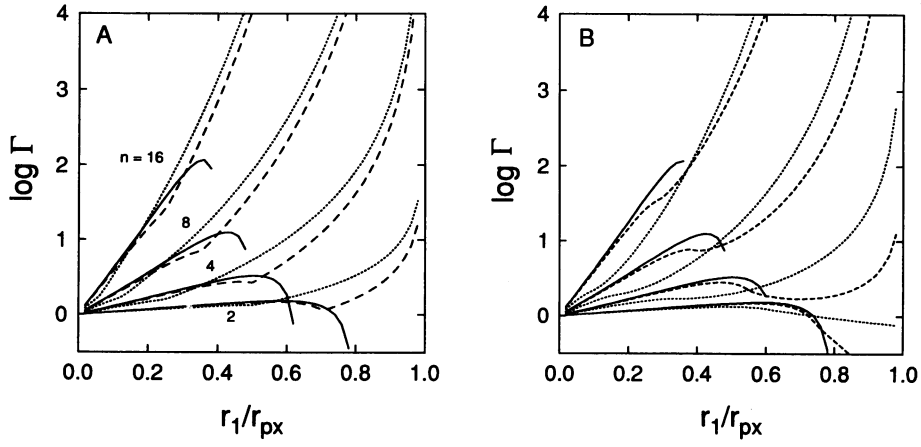

FIGURE 2 Log Γ for formation of dimers, tetramers, octamers, and hexadecimers plotted as a function of the ratio of the radius or pseudo-radius of monomer to the halfwidth of a planar pore. The results of hard particle ($W_{uv} = 0$) calculations are shown for the formation of compact n-mer (——), rod-like n-mer (· · · · ·), and plate-like n-mer (- - - -). (*A*) Results obtained with orientations discretized as described in text. (*B*) Results of Minton (1992), obtained for all possible orientations.

a single boundary surface. W_{uv}, the general surface area dependent well depth parameter used in the formulation of Eqs. 5–7 and 11–13, is then given by $W_{uv} = W_1 r_u r_v/(4r_1^2)$.

Soft repulsive interactions ($W_1 > 0$)

The value of log Γ for formation of a rod-like tetramer in a planar pore is plotted as a function of pore size and (repulsive) interaction potential in Fig. 3. It may be seen that as W_1 increases, the dependence of Γ on pore size varies as if the pore were slightly shrinking in width. The analogy is exact in the limit $W_{uv} \to \infty$, where the width of the pore is reduced from $2r_{px}$ to $2(r_{px} - d)$. No significant effect is observed for $r_1/r_p < 0.5$.

Weakly attractive interactions ($W_1 < 0$)

The value of log Γ for association of four cubical monomers to form each of three differently shaped tetramers is plotted as a function of pore size and the strength of particle-boundary interaction in Fig. 4 for the planar pore model, Fig. 5 for the square pore model, and Fig. 6 for the cubical pore model. The value of log Γ for association of two cubical monomers to form a rod-like dimer in a square pore is plotted as a function of pore size and the particle-boundary interaction energy in Fig. 7. The following qualitative features are noted:

1. For a given oligomer shape, pore shape, pore size, and interaction potential, Γ increases substantially with extent of oligomerization (value of n). A similar effect was noted for pure hard particle confinement effects in Part I.

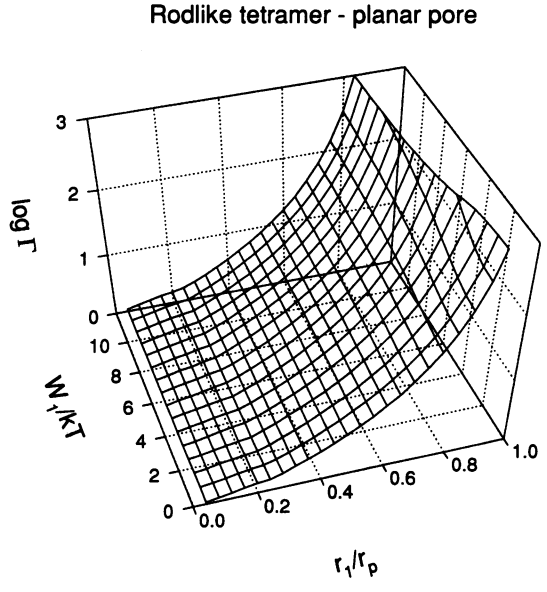

FIGURE 3 Log Γ for formation of a rod-like tetramer in a planar pore, plotted as a function of the ratio of the pseudo-radius of cubical monomer to the halfwidth of the pore, and the interaction potential W_1. The range of the interaction, d, is taken to be equal to 0.1 r_1 in this and subsequent calculations.

2. For a given oligomer shape and pore shape, Γ generally increases with increasing interaction potential and decreasing pore size (increasing r_1/r_p) until a pore becomes too small to accomodate an oligomer of the specified shape. As the size of the pore shrinks, at high interaction potentials Γ may go through a maximum and start to decrease with further pore shrinkage. Unlike the case of repulsive interactions, Γ can become large even for large pore sizes (i.e., small values of r_1/r_p) for relatively modest values of W_1.
3. For each pore shape and set of coordinates $\{W_1, r_1/r_p\}$, the value of Γ increases with oligomer shape in the order compact tetramer < plate-like tetramer < rod-like tetramer.
4. For each oligomer shape and set of coordinates $\{W_1, r_1/r_p\}$, the value of Γ increases with pore shape in the order planar pore < square pore < cubical pore.

The effect of large increases in Γ on the extent of association within a pore is illustrated by the following calculation. The composition of the bulk phase is selected to contain 1% tetramer and 99% monomer at a concentration of 1 g/l; this corresponds to an equilibrium constant $K_4^{bulk} = 0.01$ (l/g)^3. The mass fraction of tetramer in a "closed" planar pore, i.e., a pore in which the total w/v concentration of solute is held constant, and an "open" planar pore, i.e., a pore in which solute may equilibrate with the bulk, was calculated as a function of pore size and interaction potential. The results are plotted in Fig. 8, and it may be seen that in both types of pore, but particularly in the open pore, changes in W_1 as small as 6–8 k_BT may result in a 10- to 50-fold change in the fraction of solute in the pore that is present as tetramer.

To ascertain the mechanism underlying the observed large increases in Γ (as much as several orders of magnitude), the following calculation was carried out. An allowed configurational state is defined as "bound" if at least one face of the confined particle lies within distance d of a pore boundary, and defined as "free" otherwise. (Forbidden states are neither free nor bound.) Thus, Eq. 10b may be rewritten as

$$I_1(m, t) = I_1^{free}(m, t) + I_1^{bound}(m, t), \tag{22a}$$

where

$$I_1^{free}(m, t) = \begin{cases} r_{pm} - r_t - d & \text{Case I} \\ 0 & \text{Case II} \\ 0 & \text{Case III} \\ 0 & \text{Case IV} \end{cases} \tag{22b}$$

and

$$I_1^{bound}(m, t) = \begin{cases} d \cdot \exp(-W_{uv}) & \text{Case I} \\ I_1(m, t) & \text{Case II} \\ I_1(m, t) & \text{Case III} \\ 0 & \text{Case IV} \end{cases}. \tag{22c}$$

For the case of the planar pore, substitution of Eq. (22a) into Eq. (17) yields

$$\mathbf{K}_i = \mathbf{K}_i^{free} + \mathbf{K}_i^{bound}, \tag{23a}$$

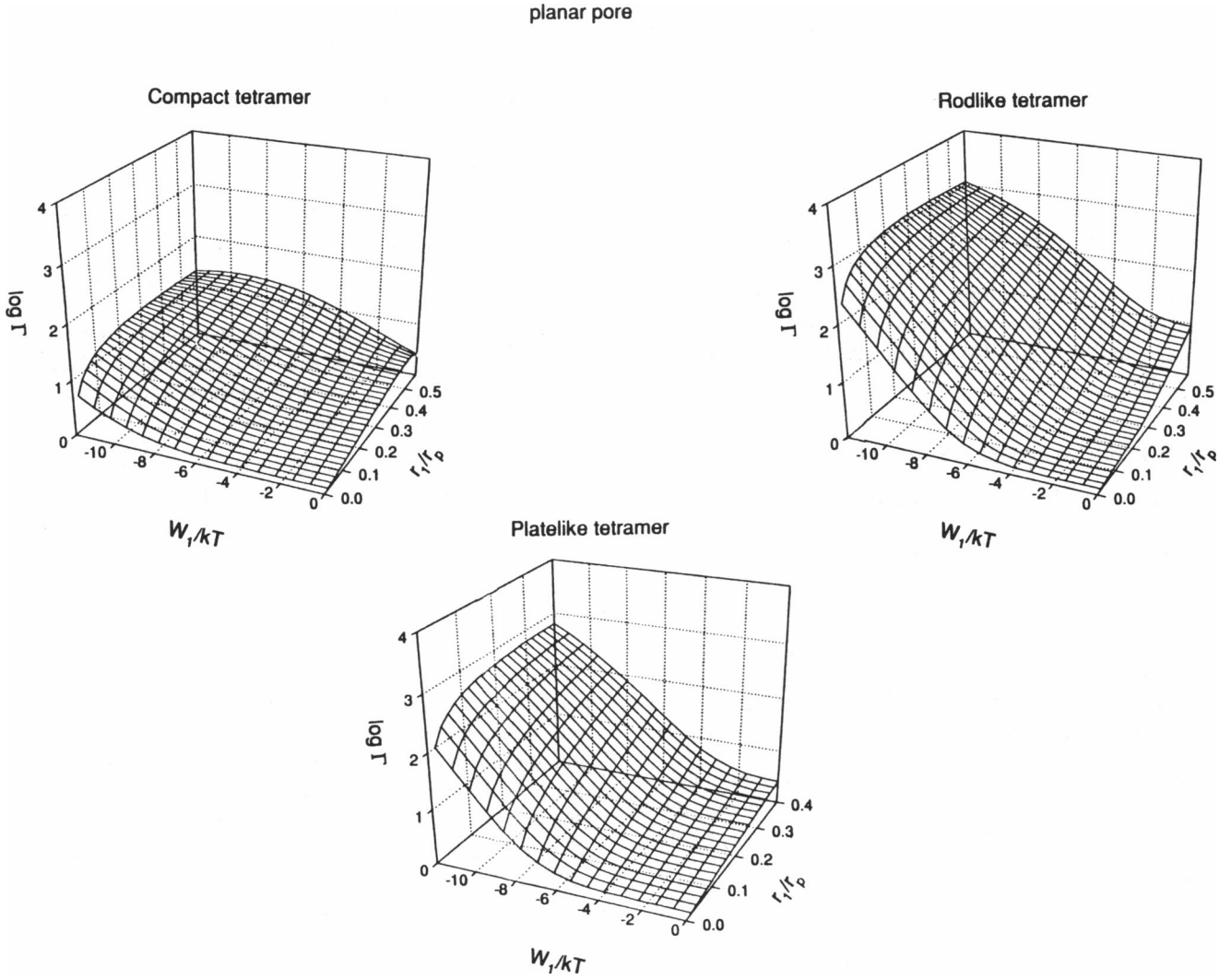

FIGURE 4 Log Γ for formation of compact, rod-like, and plate-like tetramers in a planar pore, plotted as a function of the ratio of the pseudo-radius of cubical monomer to the halfwidth of the pore and the interaction potential. Note that range of r_1/r_p axis may differ for different tetramer shapes, because different shapes have different exclusion limits.

where

$$\mathbf{K}_i^{\text{free}} = \frac{I_1^{\text{free}}(x, a) + I_1^{\text{free}}(x, b) + I_1^{\text{free}}(x, c)}{3\, r_{px}} \tag{23b}$$

and

$$\mathbf{K}_i^{\text{bound}} = \frac{I_1^{\text{bound}}(x, a) + I_1^{\text{bound}}(x, b) + I_1^{\text{bound}}(x, c)}{3\, r_{px}}. \tag{23c}$$

One can now calculate the relative w/v concentrations of free monomer, bound monomer, free n-mer, and bound n-mer:

$$w_i^{\text{free}} = \mathbf{K}_i^{\text{free}}\, w_i^{\text{bulk}} \qquad w_i^{\text{bound}} = \mathbf{K}_i^{\text{bound}}\, w_i^{\text{bulk}} \tag{24}$$

The mass fraction of each species is given by

$$f_i^{\text{free}} = w_i^{\text{free}}/\Sigma \qquad f_i^{\text{bound}} = w_i^{\text{bound}}/\Sigma \tag{25}$$

where

$$\Sigma \equiv \sum_j (w_j^{\text{free}} + w_j^{\text{bound}})$$

Consider a solution containing 1 g/l solute that self-associates to form tetramer with an equilibrium constant $K_4 = 8$ l/g. At this concentration, 50% by mass of the solute is monomer and 50% is tetramer. Let this solution equilibrate with a planar pore. The mass fraction of solute in each of the states defined above within the pore, calculated as described above, is plotted as a function of the ratio of monomer size to pore dimension in Fig. 9 for three different interaction potentials. In Fig. 10 the total w/v concentration of solute in the pore is plotted as a function of pore size for each of the three different interaction potentials. The major qualitative features are as follows. The ratio of free tetramer to free

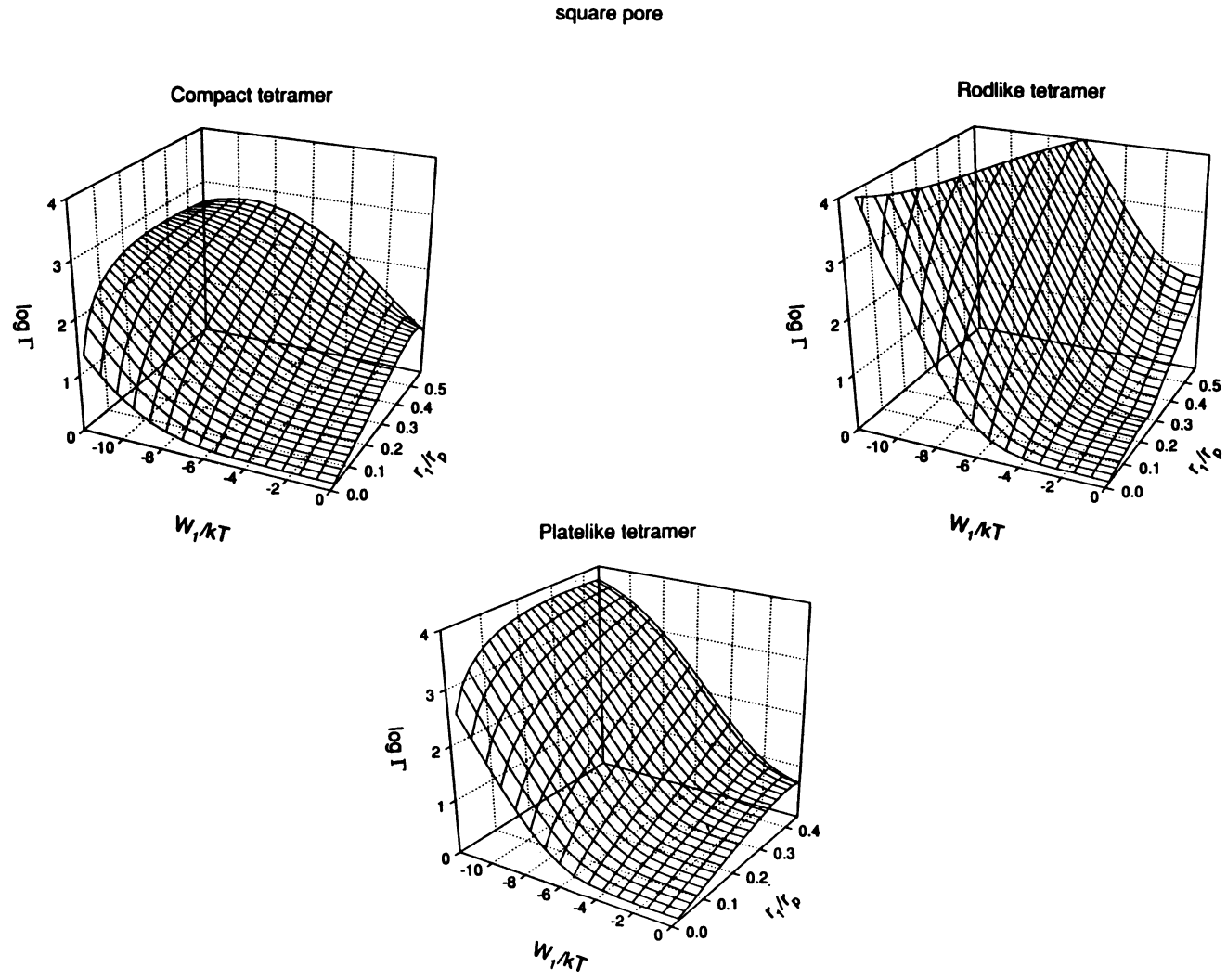

FIGURE 5 Log Γ for formation of compact, rod-like, and plate-like tetramers in a square pore.

monomer remains roughly equal (within a factor of 2) to the bulk ratio of tetramer to monomer over the range of the calculation (pore width $\geq$ 2.5 monomer pseudo-diameter). However, the ratio of bound tetramer to bound monomer is strongly dependent on interaction potential and pore size; as the interaction potential becomes more negative, bound tetramer becomes the dominant solute species within the pore, and does so at increasingly larger pore sizes (smaller values of r_1/r_p). The results shown in Fig. 10 indicate that in the absence of an attractive interaction between solute particles and pore boundaries ($W_1 = 0$) solute is excluded as the pore size decreases relative to the size of monomer; this result was noted in Part I. However, when the interaction potential becomes sufficiently large ($W_1 < \sim -4\ k_BT$) solute preferentially distributes into the pore. The results shown in Fig. 9 reveal that this is due to adsorption of oligomeric solute onto the pore boundaries.

The standard Helmholtz free energy of adsorption of the ith species from the bulk phase is given by

$$\Delta A_i^\circ = -k_B T \ln \mathbf{K}_i^{\text{bound}} \qquad (26)$$

The standard free energies of adsorption of four cubical monomers and one rod-like tetramer in a planar pore are plotted as functions of pore size and interaction potential in Fig. 11. For a given combination of W_1 and r_1/r_p, the adsorption free energy for tetramer is of the order of 10–15 k_BT more negative than that for four monomers. Because the energy changes of the two processes are identical, the difference is entirely attributable to a more favorable (negative) value of $-T\Delta S$ for the tetramer than for the four monomers.

These observations may be rationalized in the context of the thermodynamic cycle depicted schematically in Fig. 12. When attractive interactions between particles in the pore and the pore boundary surface are sufficient to result in a significant extent of adsorption, adsorption of the oligomer is substantially favored because of a smaller loss of entropy associated with the adsorption of one tetramer relative to that of four monomers. Both tetramerization of free monomers and adsorption of monomers (that is, the upper and left-hand equilibria of the cycle) require an "up-front" cost in negentropic work of co-localization. As a result, less negentropic

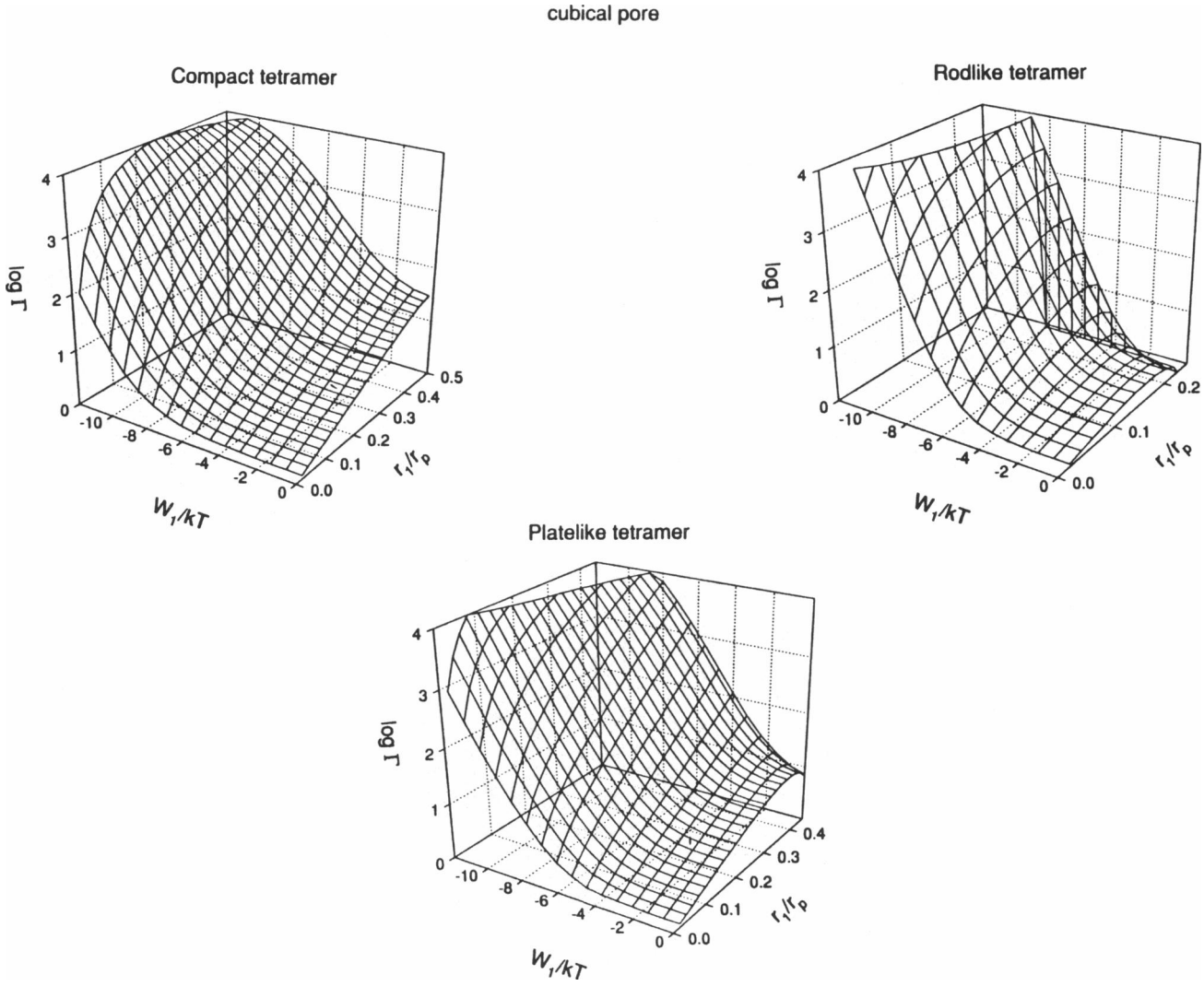

FIGURE 6 Log Γ for formation of compact, rod-like, and plate-like tetramers in a cubical pore.

work of co-localization is required to complete the formation of bound tetramers, either by tetramerization of bound monomers or by the adsorption of free tetramers (the lower and right-hand equilibria of the cycle). A sufficiently attractive potential of interaction between particles in solution and the pore boundary provides the energetic means for overcoming the initial entropy barrier to adsorption.

It was observed that enhancement of oligomerization is increased as one progresses from the planar to the square and again to the cubical pore models. This observation may be understood as reflecting the added stability of particles that can simultaneously engage in interactions with two boundaries of a square pore (i.e., lying near the corners of the square) and with three boundaries of a cubical pore (lying near the corners of the cube). If these maximally interacting states dominate the thermodynamics of association in their respective pores, log Γ should roughly scale as the negative of the interaction energy of the maximally interacting state, proportional to the interacting surface area of that state given in Table 1. Comparison of the numbers in this table with the

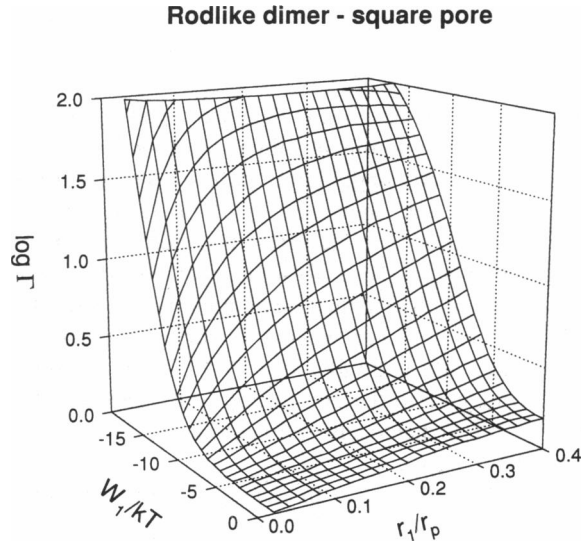

FIGURE 7 Log Γ for formation of a rod-like dimer in a square pore. Axes as in Figs. 4–6.

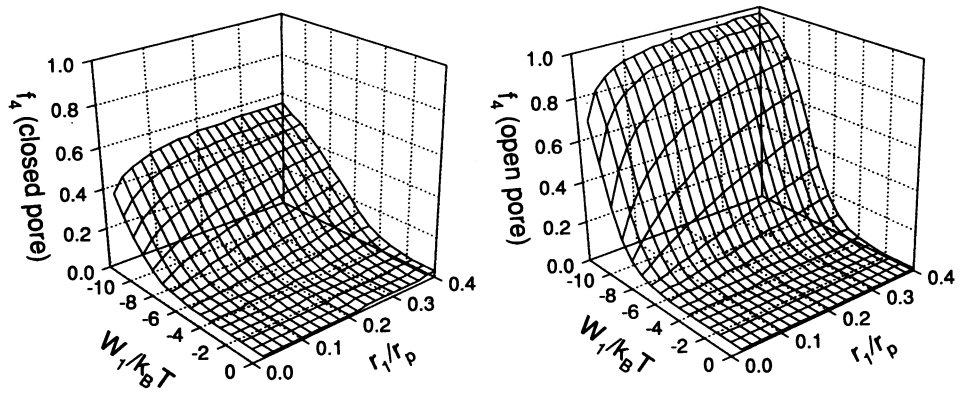

FIGURE 8 Mass fraction of rod-like tetramer in a closed planar pore (*left*) and in an open planar pore (*right*), plotted as a function of pore size and interaction potential.

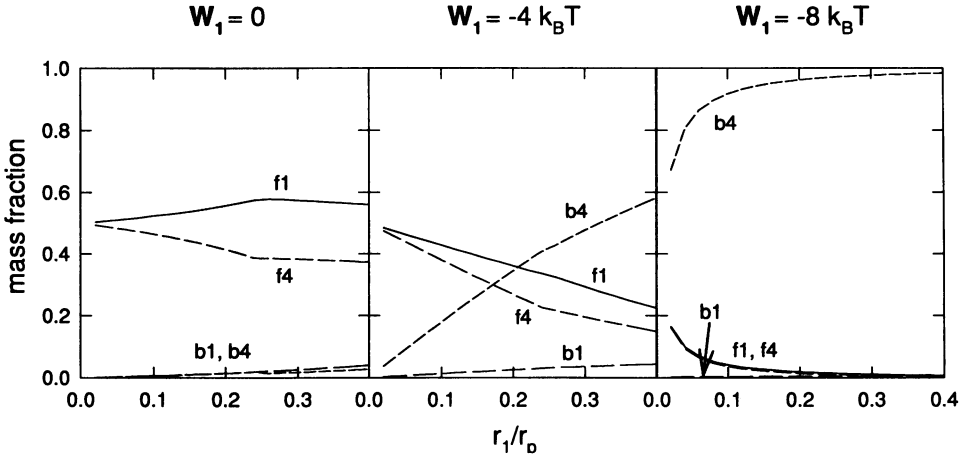

FIGURE 9 Composition of solute within a planar pore in equilibrium with bulk solution, plotted as a function of r_1/r_p for $W_1 = 0$ (*left*), $-4k_BT$ (*middle*) and $-8k_BT$ (*right*). f1, f4, b1, and b4 denote free monomer, free tetramer, bound monomer, and bound tetramer, respectively.

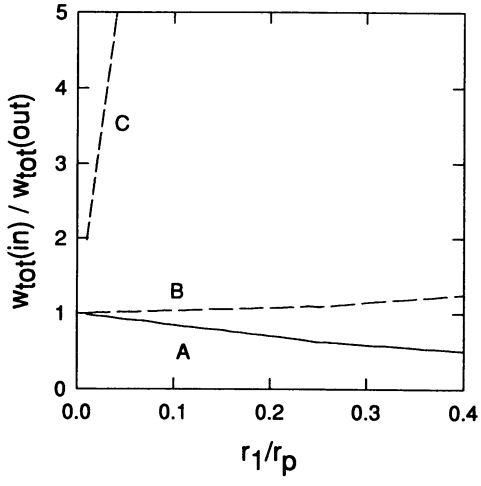

FIGURE 10 Ratio of total solute concentration inside a planar pore to that outside the pore, calculated for $W_1 = 0$ (*A*), $-4k_BT$ (*B*), and $-8k_BT$ (*C*), as a function of r_1/r_p.

functions plotted in Figs. 4–6 indicate that the relative surface areas of maximally interacting states correlate well with the relative magnitudes of log Γ for formation of differently shaped oligomers in differently shaped pores.

An interesting prediction arising from this analysis is that as the pore shrinks toward the size of the monomer, the entropy of the free monomer will decrease and the transition between free and bound states will be dominated more by energetic than negentropic contributions to the free energy. For example, because one tetrameric cube has less maximally interacting surface in a square pore than have four monomeric cubes, one might expect that as energetic changes become larger and begin to dominate the overall free energy change for formation of compact tetramers in a square pore, log Γ should go through a maximum and start to decrease. The results plotted in Fig. 13 reveal that this is indeed the case.

ISOMERIZATION REACTION

Consider the isomerization modeled by the following constant volume reaction:

$$PP(1 \times 1 \times 1) \rightleftharpoons PP(f^{2/3} \times f^{-1/3} \times f^{-1/3})$$

The particle on the left-hand side is a cube, and the particle on the right-hand side is a parallelopiped of square cross section with an axial ratio of f; it is rod-like if $f > 1$ and plate-like if $f < 1$. Let the isomerization in the bulk (unconfined) phase be characterized by an equilibrium

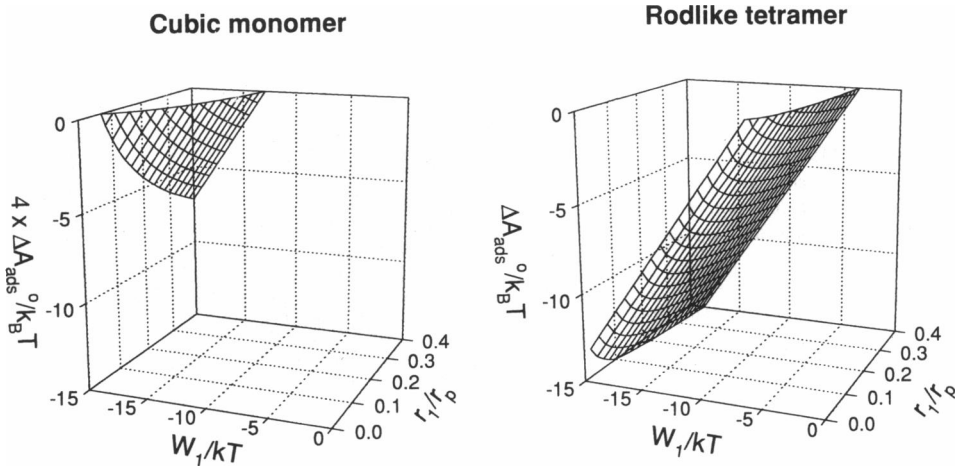

FIGURE 11 Calculated standard free energy changes associated with the adsorption of four molecules of monomer (*left*) and one molecule of rod-like tetramer in a planar pore, plotted as functions of the interaction potential and size of the pore relative to the size of monomer.

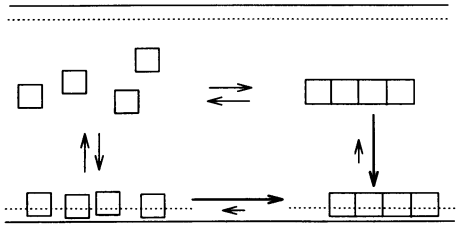

FIGURE 12 Thermodynamic cycle of equilibria between free monomer (*upper left*), free tetramer (*upper right*), bound monomer (*lower left*), and bound tetramer (*lower right*) in a planar pore. Dashed lines represent the range of the interaction.

TABLE 1 Maximum areas of particle surface interacting with pore boundaries

	Planar pore	Square pore	Cubical Pore
Cube (1 × 1 × 1)	1	2	3
Cube ($4^{1/3} \times 4^{1/3} \times 4^{1/3}$)	$4^{2/3} = 2.52$	$2 \times 4^{2/3} = 5.04$	$3 \times 4^{2/3} = 7.56$
Rod (4 × 1 × 1)	4	4 + 4 = 8	4 + 4 + 1 = 9
Plate (2 × 2 × 1)	4	4 + 2 = 6	4 + 2 + 2 = 8

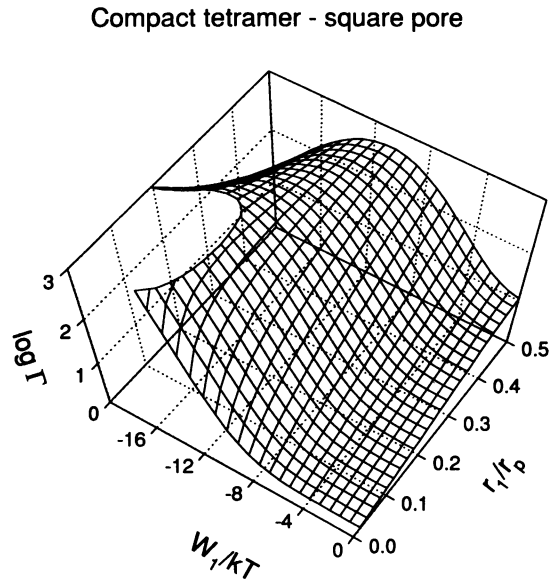

FIGURE 13 Log Γ for formation of a compact (cubic) tetramer in a square pore, plotted as a function of W_1 and r_1/r_p. These results represent the results of calculations identical to those shown in Fig. 5 extended to higher attractive interaction energy.

constant $K_{iso}^{bulk}(f)$ and the standard free energy change $\Delta A_{iso}^{bulk}(f) = -RT \ln K_{iso}^{bulk}(f)$. Then it follows from Eq. 1 that

$$\Gamma(f) \equiv K_{iso}^{pore}(f)/K_{iso}^{bulk}(f) = \mathbf{K}(f)/\mathbf{K}(1) \qquad (27)$$

where K(f) is the partition coefficient for the parallelopiped of axial ratio f and

$$\Delta A_{iso}^{pore}(f) = \Delta A_{iso}^{bulk}(f) - RT \ln \Gamma(f) \qquad (28)$$

In Fig. 14 the dependence of $\Delta A_{iso}^{pore}(f) - \Delta A_{iso}^{bulk}(f)$ upon f and pore size in a planar pore is plotted for the case of no interaction and moderate interaction. In the absence of interaction between the particle and the walls of the pore, no significant effect of confinement upon isomerization is observed for $r_1/r_p \leq 0.4$. However, if there exists an attractive potential of $8k_BT$ per unit "contact" area, then conformations that maximize contact area are significantly favored: in the case of the planar pore, the equilibrium for formation of the plate-like PP is most favored, even at very large pore sizes. Note that at any pore size $\Delta A_{iso}^{pore}(f) - \Delta A_{iso}^{bulk}(f)$ is maximal at $f = 1$ (the cubical conformation), where contact area is minimized. If there existed a repulsive potential of interaction between the surface of the particle and the pore wall, then $\Delta A_{iso}^{pore}(f) - \Delta A_{iso}^{bulk}(f)$ would be minimized at $f = 1$.

At a zero-order level of approximation, one might consider the various conformations of the PP considered above to represent different possible conformations of a protein. Many globular proteins have compact quasi-spherical native conformations in solution, in which the surface area per unit

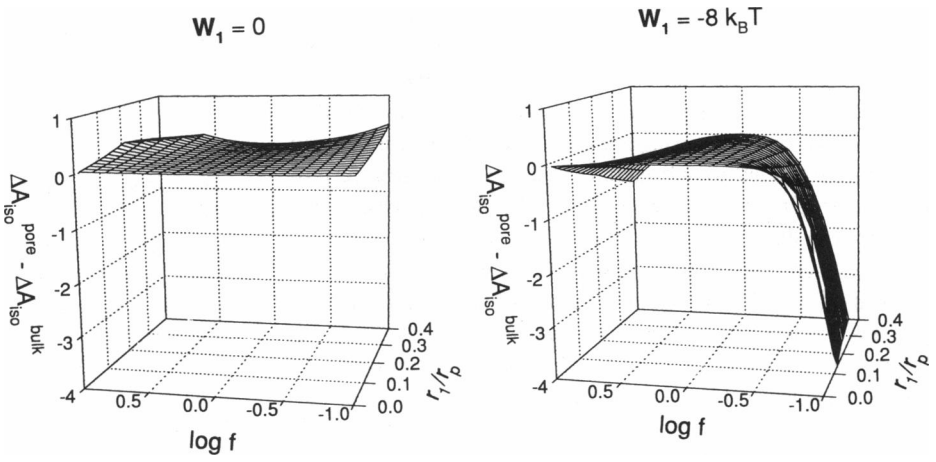

FIGURE 14 Difference between the free energy of isomerization in the planar pore and in the bulk, plotted as a function of the shape parameter f and the size of the pore relative to the size of the compact cube ($f = 1$). (*left panel*) $W_1 = 0$; (*right panel*) $W_1 = -8k_BT$.

volume is nearly minimized (Richards and Lim, 1993). This compact, native conformation is generally regarded as being associated with a global free energy minimum. Thus, distortion of the conformation in the bulk phase toward increasingly anisometric forms would be expected to result in an increase in the free energy of the protein relative to that of the global minimum, but local free energy minima are likely to exist (Frauenfelder et al., 1991), as depicted schematically in Fig. 15. The calculation presented above suggests that to the extent that nonspecific attractive forces exist between the boundaries of a pore and the surface of a protein, the free energy of a protein in the pore will contain an extra contribution, equal to $-RT \ln \Gamma(f)$ in Eq. 28, that decreases roughly monotonically with increasing anisometricity of the protein, i.e, with increasing contact surface area. Thus, the total free energy of the confined protein may have global or local minima at conformations other than the maximally compact conformation corresponding to the native state in bulk solution; this possibility is depicted schematically in Fig. 15.

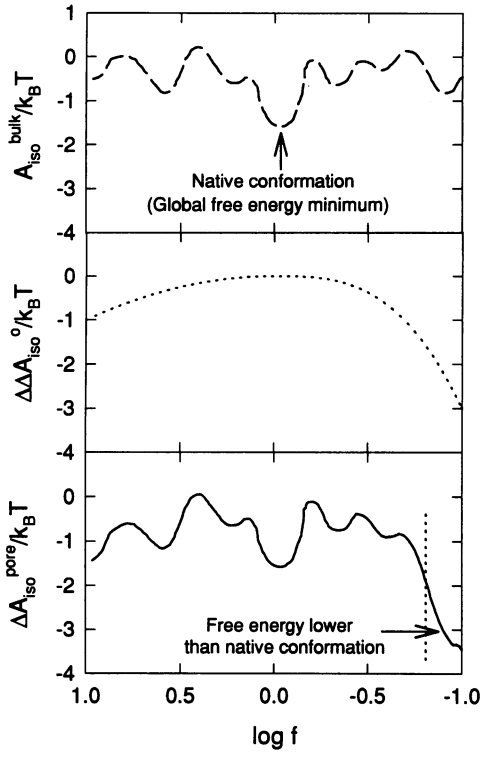

FIGURE 15 Schematic depiction of the free energy of conformational change of a protein as a function of axial ratio in the absence of surface interaction (*top*) and in the presence of attractive surface interaction (*bottom*). The difference between the two free energy plots, plotted in the central panel, has a functional form chosen to resemble qualitatively the difference function plotted in the right panel of Fig. 14.

POSSIBLE RELEVANCE TO CELL BIOLOGY

The results reported here indicate that weak, nonspecific attractive potentials acting between the boundaries of a confining volume element and confined macromolecules can result in qualitative enhancement of the extent of association of the confined macromolecules as well as possible alteration of the minimum energy conformation. The attractive potentials at which substantial effects are observed are as small as 4–8 k_BT (2.5–5 kcal/mol at room temperature), i.e., of the order of magnitude of hydrogen bonds, hydrophobic interactions, or simple attraction between charged or partially charged groups in aqueous solution (Némethy et al., 1963; Rose and Wolfenden, 1993).

We have experimentally observed presumably nonspecific associations between unrelated globular proteins and fibrous actin in solutions of moderate ionic strength (Lakatos and Minton, 1990). These associations are characterized by standard free energy changes of the order of $-10\,RT$ per mole of globular protein, where $R = k_B \times$ Avogadro's number. Although the models used here are too simple to be compared quantitatively with experiment, the results shown in Fig. 11 suggest that free energy changes of this magnitude could reflect substantially more negative energies or enthalpies of interaction, a hypothesis that may of course be tested experimentally. If this proves to be the case, one might expect the nonspecific association of globular proteins with extended substrates such as F-actin to be accompanied by extensive self- or heteroassociation of adsorbed protein.

To the extent that adsorption does not intrinsically interfere with association of a particular pair of soluble protein species (by, for example, requiring the participation of a particular surface region of the protein that would otherwise be involved in the formation of a heterocomplex of soluble proteins), adsorption would be expected to substantially enhance any intrinsic propensity for self- or heteroassociation of the globular species that may exist in the absence of the adsorbing substrate. The results presented here thus tend to support the view of eukaryotic cytoplasm proposed by Clegg (1984), according to which soluble proteins are in the main present as complexes adsorbed onto fibrous structural elements such as actin fibers. Because adsorption is expected to be (or perhaps defined to be) largely nonspecific, the composition of adsorbed protein complexes would reflect the intrinsic relative affinity of each species of soluble protein for itself and each of the other species present, differences in the adsorption tendency of each species, and the total concentration of each species in the cytoplasm.

I thank Dr. William Gelbart, UCLA, for critically reviewing an early draft of this report.

REFERENCES

Clegg, J. S. 1984. Properties and metabolism of the aqueous cytoplasm and its boundaries. *Am. J. Physiol.* 246:R133–R151.

Frauenfelder, H., S. L. Sligar, and P. G. Wolynes. 1991. The energy landscapes and motions of proteins. *Science.* 254:1598–1603.

Giddings, J. C., E. Kucera, C. P. Russell, and M. N. Myers. 1968. Statistical theory for the equilibrium distribution of rigid molecules in inert porous networks: exclusion chromatography. *J. Phys. Chem.* 72:4397–4408.

Hirokawa, N. 1991. Molecular architecture and dynamics of the neuronal cytoskeleton. *In* The Neuronal Cytoskeleton. R. D. Burgoyne, editor. Wiley-Liss, New York. 5–74.

Lakatos, S., and A. P. Minton. 1990. Interactions between globular proteins and F-actin in isotonic saline solution. *J. Biol. Chem.* 266:18707–18713.

Leiken, S., D. C. Rau, and V. A. Parsegian. 1994. Direct measurement of forces between self-assembled proteins: temperature-dependent exponential forces between collagen triple helices. *Proc. Natl. Acad. Sci. USA.* 91:276–280.

Minton, A. P. 1992. Confinement as a determinant of macromolecular structure and reactivity. *Biophys. J.* 63:1090–1100.

Muramatsu, N., and A. P. Minton. 1989. Hidden self-association of proteins. *J. Mol. Recog.* 1:166–171.

Némethy, G., I. Z. Steinberg, and H. A. Scheraga. 1963. Influence of water structure and hydrophobic interactions on the strength of side-chain hydrogen bonds in proteins. *Biopolymers.* 1:43–69.

Porter, K. R. 1984. The cytoplasmic matrix and the integration of cellular function: proceedings of a conference. *J. Cell Biol.* 99.

Richards, F. M., and W. A. Lim. 1993. An analysis of packing in the protein folding problem. *Q. Rev. Biophys.* 26:423–498.

Rose, G. D., and R. Wolfenden. 1993. Hydrogen bonding, hydrophobicity, packing, and protein folding. *Annu. Rev. Biophys. Biomol. Struct.* 22: 381–415.